CrossMark

Precursor-directed synthesis of porous cobalt assemblies with tunable close-packed hexagonal and face-centered cubic phases for the effective enhancement in microwave absorption

Ying Wang[1], Yunchen Du[1,*], Di Guo[1], Rong Qiang[1], Chunhua Tian[1], Ping Xu[1], and Xijiang Han[1,*]

[1] *MIIT Key Laboratory of Critical Materials Technology for New Energy Conversion and Storage, School of Chemistry and Chemical Engineering, Harbin Institute of Technology, Harbin 150001, China*

ABSTRACT

Metal cobalt is one of the most promising candidates for high-performance microwave absorbers due to its compatible dielectric loss and magnetic loss abilities. Rational design on the microstructure of metal cobalt became a popular way to upgrade its microwave absorption performance in the past decade, while much less attention has been paid to the electromagnetic functions derived from its different crystal structures. Herein, we report the microwave absorption of porous cobalt assemblies with varied composition of close-packed hexagonal (hcp) and face-centered cubic (fcc) phases. Electromagnetic analysis reveals that the change of phase composition can significantly impact the complex permittivity and complex permeability of metal cobalt, where hcp-cobalt favors high complex permittivity and fcc-cobalt produces high complex permeability. The optimum phase composition in these porous cobalt assemblies will promise well-matched characteristic impedance and good performance in strong reflection loss (−41.0 dB at 9.4 GHz) and wide response bandwidth (4.0–17.4 GHz over −10.0 dB). The enhanced microwave absorption is superior to many cobalt absorbers ever reported. It is believed that these results will provide a new pathway to the design and preparation of highly effective metal cobalt and cobalt-based composites as novel microwave absorbers in the future.

Introduction

In the past decades, metal cobalt, as a typical magnetic material, has received a great deal of attention because of its wide range of applications in magnetic storage, permanent magnets, catalysis, superalloys, cemented carbides, etc. [1–5]. Recent progress indicates that the large saturation magnetization and high Snoek's limit in the gigahertz range, as well as the compatible dielectric loss property also render metal cobalt as a promising candidate for high-performance

Address correspondence to E-mail: yunchendu@hit.edu.cn; hanxijiang@hit.edu.cn

🌀 Springer

microwave absorbing materials, which can effectively regulate the excessive electromagnetic interference and electromagnetic pollution caused by rapidly expanded applications of communication technology in both civil and military fields [6–8]. Metal cobalt has long been known to have three crystal structures, namely, close-packed hexagonal (hcp), face-centered cubic (fcc), and primitive cubic phases (ε phase), where hcp and fcc are two stable forms for bulk metal cobalt [9]. In general, hcp-cobalt and fcc-cobalt can coexist at room temperature, while the fcc structure is thermodynamically preferred above 450 °C, and the hcp phase is favored at lower temperatures [10]. Although hcp-cobalt and fcc-cobalt are both close-packed structures that differ only in the stacking sequence of atomic planes in the 111 direction, their electronic and magnetic properties are remarkably distinguishable. For example, the Fermi energies of hcp-cobalt and fcc-cobalt are 5.49 and 5.29 eV, respectively, and hcp-cobalt also possesses higher electron density around the Fermi level than fcc-cobalt [11]; the electron localization function of hcp-cobalt is a radial electron distribution, while fcc-cobalt electron distribution has evident polarization [11]. On the other hand, the difference in bulk anisotropy between hcp-cobalt [K_1(hcp) = 5.0×10^6 erg/cm^3] and fcc-cobalt [K_1(fcc) = 0.8×10^6 erg/cm^3] also leads to their different magnetic coercivity [10, 12]. In view of these facts, it is expected that tuning the crystal phases of cobalt nanoparticles may change their electromagnetic properties and microwave absorption. Previous papers reported the microwave absorption of metal cobalt with single hcp phase or mixed hcp–fcc phase [13–15]; however, the contribution of tunable phase compositions has not been systematically investigated yet.

Instead of tuning the intrinsic properties of metal cobalt, most researchers showed their special interests in constructing unique microstructures of metal cobalt to improve its microwave absorption performance [16–20]. For example, Liu et al. investigated the electromagnetic properties of cobalt microspheres and cobalt dendrites, and they found that cobalt dendrites showed better dielectric loss ability and consequent reflection loss characteristics [16]; Wen et al. obtained spherical, chain-like, and flake-like cobalt powders with similar crystal structures, where chain-like and flake-like cobalt powders exhibited their own advantages in dielectric loss ability and magnetic loss ability, respectively [17]. He et al.

confirmed that porous network was vital for the enhancement of microwave absorption, since porous materials had better impedance matching with free space than the corresponding solid materials, and porous microstructure was available for suppressing the eddy current loss of metallic magnets and maintaining high permeability [18]. The microstructure-dependent electromagnetic functions of metal cobalt intensively stimulate the rational design on the assembly of cobalt nanoparticles to achieve preferable performance in microwave absorption. Nowadays, various hierarchical cobalt assemblies, e.g., microspheres, microflowers, nanoflakes, nanowires, aligned nanofibres, dendrites, are frequently constructed and employed as effective microwave absorbers [13–26]. Although these successful examples have made significant achievements, it is actually difficult to direct/control the assembly of metal cobalt nanoparticles, because the forces between the particles caused by electron affinity, surface tension, van der Waals forces, and magnetic dipole interactions will be large [1]. In order to alleviate the agglomeration of cobalt nanoparticles, common strategies for metal cobalt with expected microstructure are generally carried out under the condition of dilute Co^{2+} concentration (<0.1 mol/L) and the assistance of organic surfactants or complexing agents [13, 19–21, 24–26]. Moreover, the experimental parameters, including reaction temperature, reaction time, and reagent dosages, must be precisely controlled, which can also affect the final microstructure of metal cobalt sensitively [19, 22, 26]. Therefore, developing a simple and scalable synthetic method for metal cobalt with specific microstructure is still a challenging task.

In recent years, precursor-directed synthesis has appeared as a quite attractive methodology for the preparation of various functional nanomaterials. This novel method exhibits unique advantages in avoiding some insuperable difficulties in the direct synthesis of the final products, and generally, the as-obtained products retain the basic morphology and structure of the precursors and show considerable improvements in their own properties [27–29]. Liu's group previously produced hollow porous cobalt absorbers with good microwave absorption properties from the precursors of Co(OH)$_2$ microspheres and CoCO$_3$ microrods, respectively [18, 30]. However, the precursors were still from the low-yield and time-consuming hydrothermal route, and more

complicatedly, $CoCO_3$ had to be firstly converted into Co_3O_4 and then reduced to metal cobalt. In this article, we demonstrate the synthesis of porous cobalt assemblies by choosing cobalt oxalate (CoC_2O_4) as the precursor, where CoC_2O_4 was pre-prepared by a simple and fast precipitation method. The composition of hcp and fcc phases is easily tunable through manipulating the temperature of hydrogen reduction. For the first time, the electromagnetic properties and microwave absorption of these cobalt assemblies with different phase compositions are analyzed carefully, and it is found that hcp and fcc phases have distinguishable contributions to dielectric loss and magnetic loss, respectively. When hcp and fcc phases were well integrated, the optimum porous cobalt assemblies would promise desirable microwave absorption, and their performance was superior to many metal cobalt absorbers previously reported. These results not only provide a simple route for preparing metal cobalt with porous structure, but also validate the importance of optimizing the intrinsic properties of metal cobalt in microwave absorption, which may be greatly helpful for the design and fabrication of high-performance cobalt-based microwave absorbers in the future.

Experimental

Synthesis

All chemical reagents are of analytical grade and used as received without any further purification. In a typical run for CoC_2O_4 precursor, 100 mL of saturated sodium oxalate solution was pre-prepared in a flask at room temperature (20 °C), and then 7.60 g of $Co(NO_3)_2 \cdot 6H_2O$ powder was added into the sodium oxalate solution under vigorous mechanical stirring. After 15 min, the pink precipitate was collected by centrifugation, washed with ultrapure water and anhydrous ethanol for several times, and subsequently dried at 60 °C overnight. To obtain porous cobalt assemblies, the as-prepared CoC_2O_4 precursor was reduced in a horizontally tubular furnace under mixed H_2/N_2 ($V/V = 5:95$) atmosphere at the required temperature for 10 h with a heating rate at 1 °C/min. The final samples were denoted as Co-x, in which x represented the final reduction temperature.

Characterization

Scanning electron microscope (SEM) images were obtained on a Quanta 200S (FEI), and the samples were mounted on aluminum studs using adhesive graphite tape and sputter-coated with gold before analysis. Powder X-ray diffraction (XRD) data were recorded on a Rigaku D/MAXRC X-ray diffractometer with a CuKα radiation source (45.0 kV, 50.0 mA). High-resolution TEM (HRTEM) images were recorded by a Tecnai F20 operating at an accelerating voltage of 200 kV. The thermogravimetric analysis was carried out on a SDT Q600 TGA (TA Instruments) in the temperature range from room temperature to 800 °C at a heating rate of 10 °C/min. The magnetic hysteresis loops were made using a LakeShore 7404 (LakeShore, USA) vibrating sample magnetometer (VSM). The specific surface area was calculated on a Micromeritics ASAP 2020 using the Brunauer–Emmett–Teller (BET) method from the nitrogen adsorption data in the relative range (P/P_0) of 0.05–0.20. Samples were normally prepared for measurement by degassing at 120 °C until a final pressure of 1×10^{-3} Torr was reached. An Agilent N5230A vector network analyzer (Agilent, USA) was applied to determine the relative permeability and permittivity in the frequency range of 2.0–18.0 GHz for the calculation of reflection loss. A sample containing 70 wt% of as-prepared product was pressed into a ring with an outer diameter of 7 mm, an inner diameter of 3 mm, and a thickness of 2 mm for microwave measurement in which paraffin wax was used as the binder.

Results and discussion

The crystalline structure of the precursor is primarily studied by wide angle XRD, and as shown in Fig. S1, the characteristic diffraction peaks in the range of 15°–50° can be precisely indexed to γ-$CoC_2O_4 \cdot 2H_2O$ with a monoclinic structure ($P2_1/m$) [31]. SEM image reveals that the precursor is fully composed of flower-like assemblies with an average size of about 6.7 μm (Fig. S2), where numerous well-defined nanoneedles with diameter of 200–250 nm act as the basic units of these assemblies. This uniform microstructure provides a good platform for the in situ transformation from γ-$CoC_2O_4 \cdot 2H_2O$ to metal cobalt. Figure 1 shows the microstructure evolution

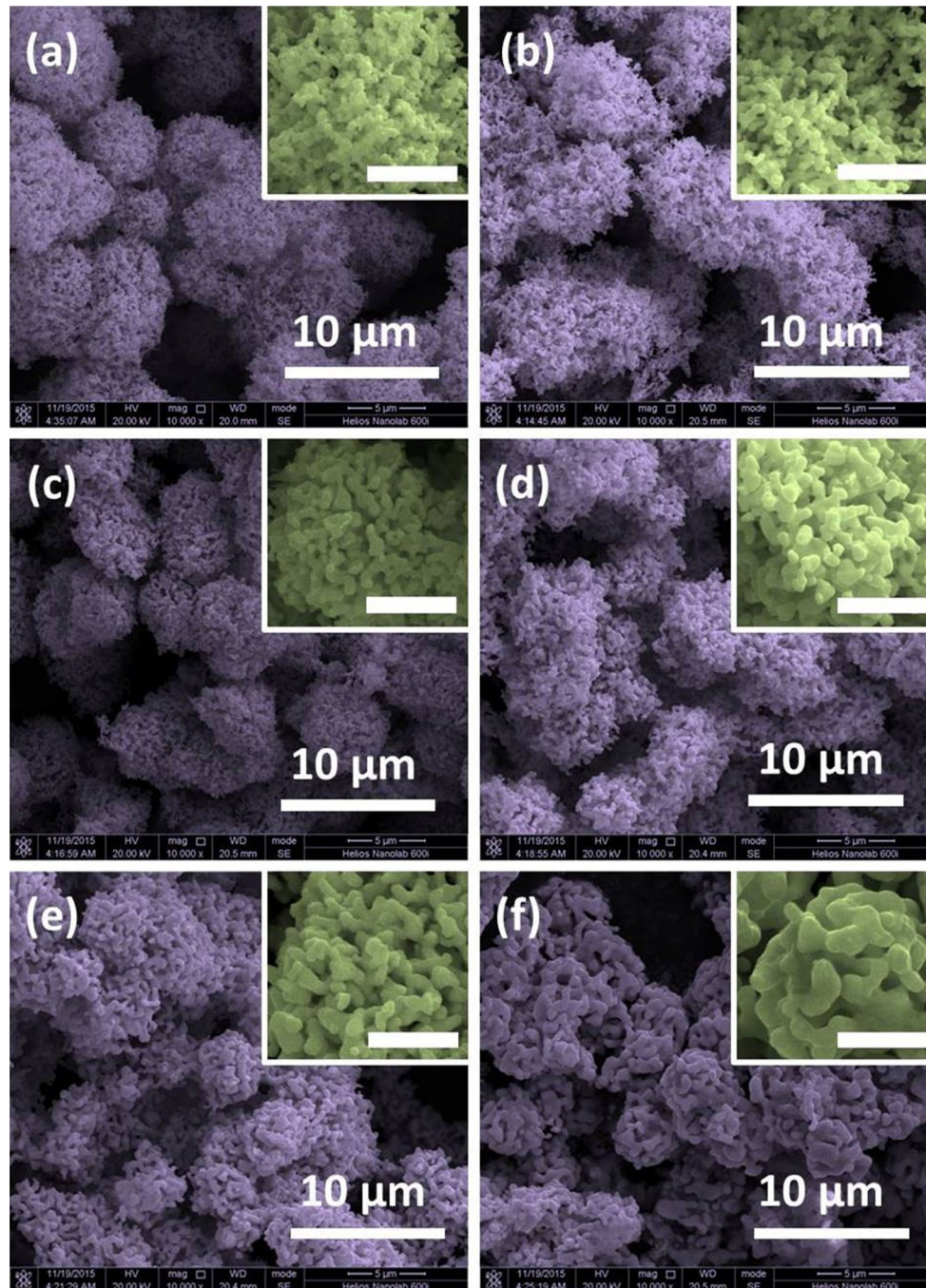**Figure 1** SEM images of Co-300 (**a**), Co-350 (**b**), Co-400 (**c**), Co-450 (**d**), Co-500 (**e**), and Co-550 (**f**). *Inset* in each SEM image is the corresponding image with improved resolution (the *scale bars* in these *insets* are 2 μm).

of metal cobalt obtained at different reduction temperatures. It is obvious that all samples exhibit quasi-spherical assemblies instead of initial flower-like assemblies and the tightly packed nanoneedles also turn into the cross-linked particles, implying that the transformation process has been effectively performed. The decomposition of the precursor accompanied with the release of gaseous species (e.g., H_2O, CO_2, CO) produces loose internal structures and abundant pores in these cobalt assemblies. According to previous reports, these porous structures are indeed favorable for promoting the attenuation of incident electromagnetic waves by multiple reflection and scattering [32, 33]. Although the

increase of the reduction temperature stimulates the growth of these particles to some extent (Fig. 1a–d, insets), the average size and microstructure of these assemblies are less impacted below 450 °C. It is possible that the phase transition from hcp to fcc may play a more progressive role than the particle growth below 450 °C, and thus the microstructure of these assemblies can be well retained in the temperature range of 300–450 °C. However, fcc phase becomes overwhelming above 450 °C [10], which means that higher temperature will only contribute to the fusion and growth of cobalt particles (Fig. 1e, f, insets). As a result, Co-500 and Co-550 present an evident shrinkage, and this change further leads to a decrease in the porosity (Fig. 1e, f). The data of BET surface and pore volume confirm the difference in the microstructure of these cobalt assemblies (Table S1). According to the results of N_2 adsorption, the values of BET surface for Co-300, Co-350, Co-400, Co-450, Co-500, and Co-550 are 7.12, 7.07, 5.92, 4.34, 1.65, and 0.33 m^2/g, respectively; the corresponding values of pore volumes are 1.24×10^{-3}, 2.26×10^{-3}, 1.87×10^{-3}, 1.50×10^{-3}, 0.89×10^{-3}, and 0.59×10^{-3} cm^3/g, respectively. It has to mention that Co-300 has similar BET surface to Co-350, but its pore volume is much smaller, which may be attributed to the incomplete decomposition or reduction of the CoC_2O_4 precursor.

Figure 2 shows the XRD patterns of porous cobalt assemblies obtained at different reaction temperatures. Co-300 exhibits five well-resolved diffraction peaks in the 2θ range of 20°–80°, where the peaks at 2θ = 41.6°, 44.4°, 47.5°, and 75.8° can be assigned to the (100), (002), (101), and (110) planes of hcp-cobalt (JCPDS No. 05-0727), respectively, and the peaks at 2θ = 44.4°, 51.6°, and 75.8° belong to the (111), (200), and (220) planes of fcc-cobalt (JCPDS No. 15-0806), respectively. It can be concluded that Co-300 contains both hcp-phase cobalt and fcc-phase cobalt; however, the overlaps between the (002) plane of hcp-cobalt and the (111) plane of fcc-cobalt, as well as the (110) plane of hcp-cobalt and the (220) plane of fcc-cobalt result in the mismatched relative intensity with standard patterns. With increasing the reduction temperature, the relative intensities of the peaks at 2θ = 41.6°, 47.5°, and 75.8° are gradually decreased, and the peak at 2θ = 51.6° gradually becomes stronger and narrower, implying that the phase composition of hcp-cobalt and fcc-cobalt in these sample is tunable. In order to better understand the phase

change, the TOPAS 4.2 software developed by Bruker Corporation is applied for the Rietveld quantitative phase analysis [34]. The overall parameters of refinement are background coefficients, cell parameters, peak shape parameters, and phase scales. The peak shapes are fitted by a pseudo-Voigt Function, and Y_{obs} and Y_{cal} are the experimental spectrum and calculated profile, respectively. According to the
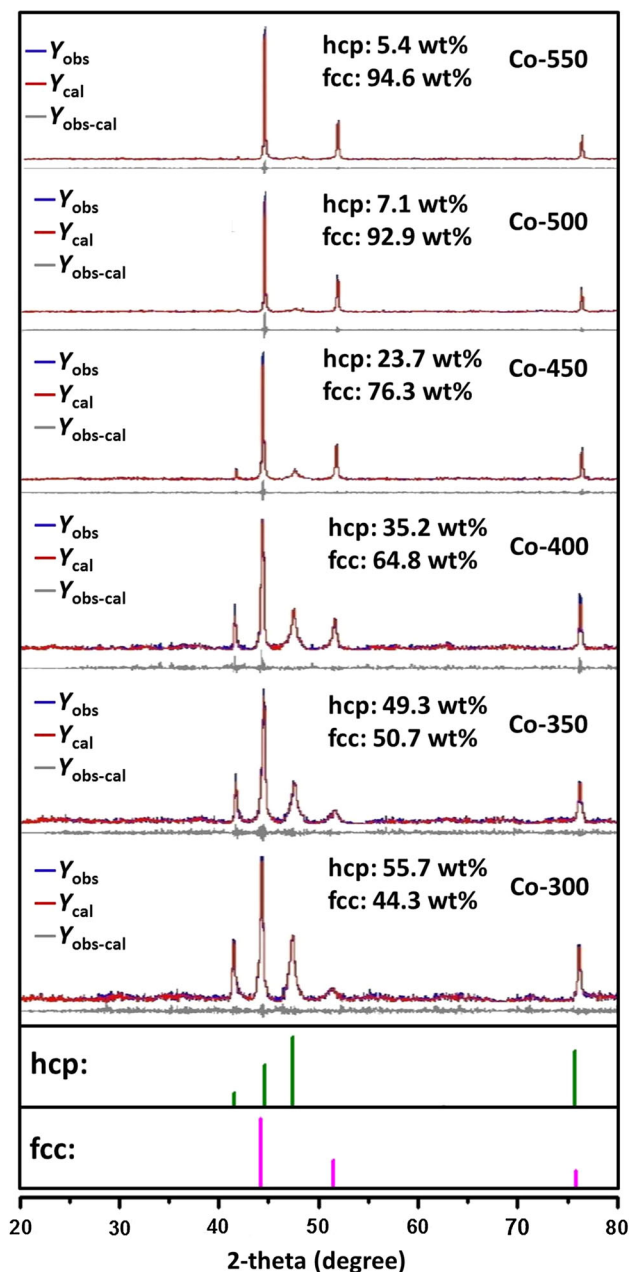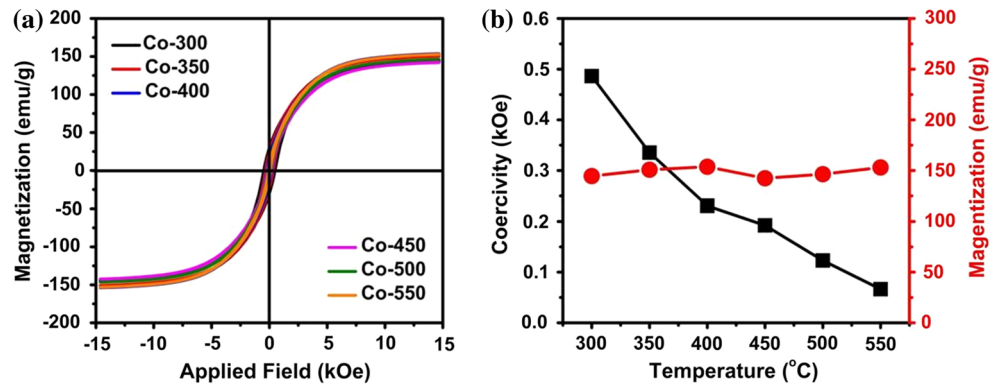

Figure 2 XRD patterns analysis by means of Rietveld refinement of Co-300, Co-350, Co-400, Co-450, Co-500, and Co-550. The Bragg positions of all the identified phases: hcp-cobalt and fcc-cobalt.

Figure 3 Magnetization hysteresis loops (**a**) and corresponding saturation magnetization and coercivity (**b**) of Co-300, Co-350, Co-400, Co-450, Co-500, and Co-550.


Rietveld refinement, the weight percentages of hcp and fcc phases are shown in Fig. 2. As expected, fcc phase gets a higher composition percentage as the reduction temperature goes up, e.g., the specific values for Co-300, Co-350, Co-400, Co-450, Co-500, and Co-550 are 44.3, 50.7, 64.8, 76.3, 92.9, and 94.6%, respectively. It is unfortunate that Co assemblies with less hcp composition cannot be created by this method due to the incomplete decomposition and reduction of the precursor at lower temperature. The slight change of phase composition at high temperature is well aligned with the proposed microstructure evolution (Fig. 1). In addition, the absence of other peaks from cobalt oxides (CoO and Co_3O_4) and CoC_2O_4 indicates the dominance of zero-valent metal cobalt in these samples. High-resolution TEM technique is further employed to characterize the microscopic connection between hcp-cobalt and fcc-cobalt by taking Co-450 as a typical sample (Fig. S3). As mentioned above, hcp-cobalt and fcc-cobalt are both close-packed structures with a small difference in the stacking sequence of 111 direction, and the preferential (002) plane in hcp-cobalt and (111) plane of fcc-cobalt have quite similar d-spacing values, and thus HRTEM image just recognizes the clear lattice fringes with d-spacing of 0.20 nm, but fails to confirm the specific assignment of different particles. However, some stacking faults can be clearly observed between two adjacent particles, which imply that hcp-cobalt and fcc-cobalt are uniformly dispersed in these cobalt assemblies with stacking faults as their interfaces, because the stacking faults usually play a crucial role in the evolution of crystalline structure of metal cobalt [12, 35]. By considering that surface oxidation of metal cobalt is a common phenomenon [10, 36], the thermogravimetric analysis is carried out to evaluate the degree of surface oxidation (Fig. S4). As heating

metal cobalt to a temperature of 800 °C in air will produce only Co_3O_4, the theoretically incremental rate of weight from metal Co to Co_3O_4 should be ca. 36 wt%. In our case, Co-350, Co-400, Co-450, Co-500, and Co-550 display quite similar incremental weight rates over 30 wt%, which suggests that surface oxidation in these samples is very limited. Compared with these samples, Co-300 not only gives a smaller incremental weight rate, but also presents a new weight loss at about 150 °C. These results illustrate that Co-300 is not sufficiently transformed and reduced as the other samples, and there are still trace impurities and few more oxides, although they are not detected by XRD.

Moreover, the effects of phase composition on the magnetic properties of these cobalt assemblies are also studied. As shown in Fig. 3a, all samples give typical ferromagnetic behaviors with very strong saturation magnetization (Ms) at about 150 emu/g. The negligible difference in Ms values can be ascribed to the pretty close magnetic moments of the hcp and fcc phases [37]. In contrast, a closer inspection reveals that the coercivity (Hc) is significantly impacted by the phase composition (Fig. S5), and the values for Co-300, Co-350, Co-400, Co-450, Co-500, and Co-600 are 486.3, 335.4, 230.7, 192.3, 123.0, and 66.5 Oe, respectively (Fig. 3b). It is widely accepted that coercivity is highly associated with particle size and magnetic anisotropy [6, 38]. On one hand, high temperatures induce the growth of Co particles, as proved by SEM images (Fig. 1), and the larger Co particles over their critical diameter (70 nm) will produce smaller coercivity [39]; on the other hand, hcp-cobalt possesses much larger magnetic anisotropy than fcc-cobalt [12], and thus the formation of high-content fcc-cobalt will also be responsible for the diminishing coercivity.

Figure 4 Real parts (**a**) and imaginary parts (**b**) of the complex permittivity, real parts (**c**) and imaginary parts (**d**) of the complex permittivity, and corresponding dielectric loss tangents (**e**) and magnetic loss tangents (**f**) of Co-300, Co-350, Co-400, Co-450, Co-500, and Co-550.
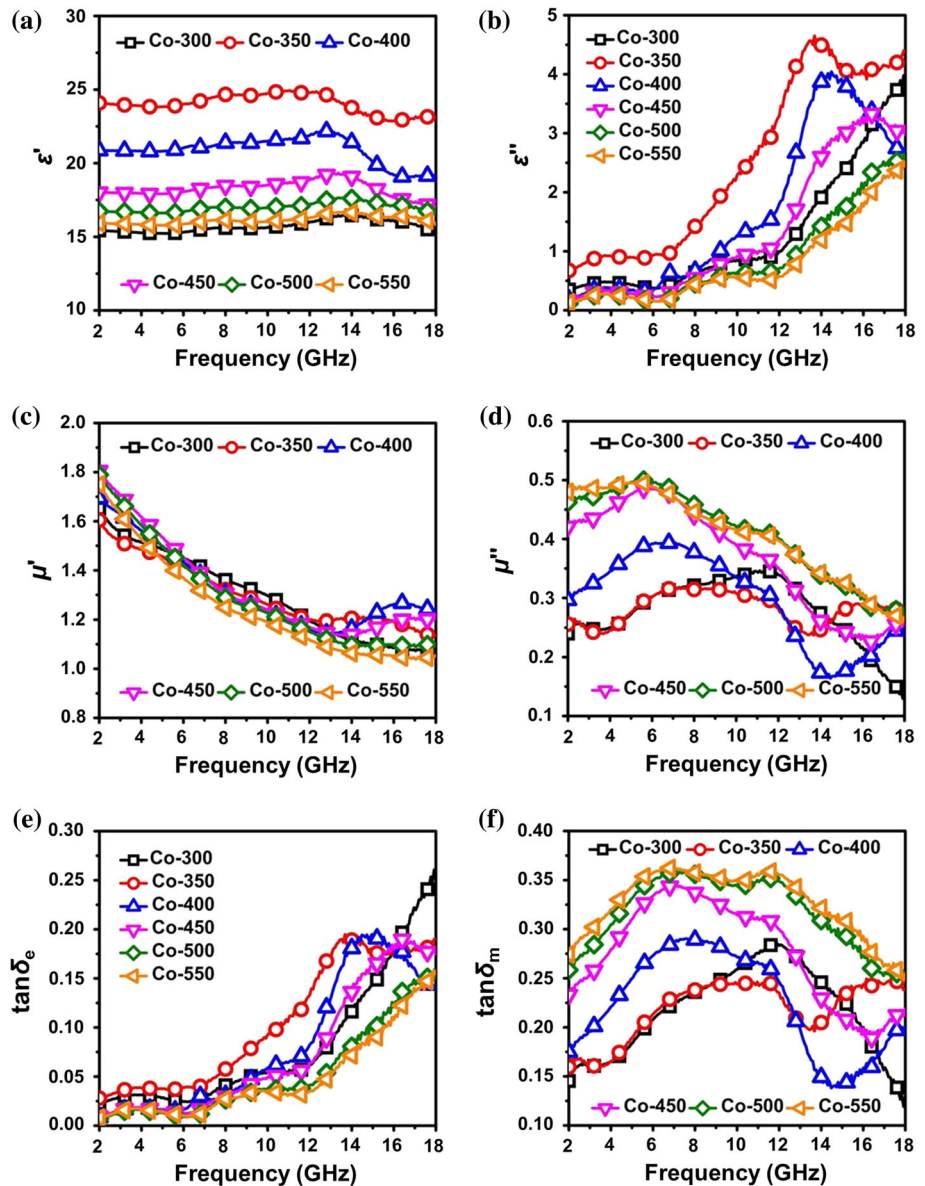
In general, complex permittivity ($\varepsilon_r = \varepsilon' - j\varepsilon''$) and complex permeability ($\mu_r = \mu' - j\mu''$) are very important parameters that can determine the microwave absorption properties of an absorber, where the real parts of complex permittivity (ε') and complex permeability (μ') represent the storage capability of electric and magnetic energy, and the imaginary parts (ε'' and μ'') describe the loss capability of electric and magnetic energy [40]. Figure 4 shows the complex permittivity and complex permeability of cobalt assemblies obtained at different temperatures in the frequency range of 2.0–18.0 GHz. As observed, the six samples display complex permittivity at different levels, demonstrating that they possess different

dielectric loss properties (Fig. 4a, b). Co-300 presents almost unchanged ε' throughout the whole frequency range, while its ε'' increases from 0.36 at 2.0 GHz to 3.84 at 18.0 GHz. Co-350 displays similar change trends in ε' and ε'' to Co-300, but their specific values are substantially enhanced, where ε' can reach about 24.0 and ε'' rises from 0.67 at 2.0 GHz to 4.40 at 18.0 GHz. With further increasing the temperature, the values of ε' and ε'' in Co-400, Co-450, Co-500, and Co-550 are gradually decreased. It is widely accepted that complex permittivity is highly associated with conductivity and polarization relaxation according to the Debye theory and free electron theory [41, 42]. As mentioned above, hcp-cobalt has higher electron

density around the Fermi level than fcc-cobalt [11], and thus hcp-cobalt can be endowed with higher electrical conductivity and consequently enhanced complex permittivity. The good consistency between the complex permittivity and the phase composition from Co-350 to Co-550 indeed confirms that the hcp-cobalt content assumes more contribution to the dielectric performance of these cobalt assemblies. Co-300 with more hcp-phase fails to promise better complex permittivity, since the presence of trace impurities and a little more oxides may pull down its conductivity. Although the electron distribution in fcc-cobalt can produce evident polarization [11], electronic polarization usually occurs at much higher frequency region (10^3–10^6 GHz) and does not work for the current electromagnetic field (2.0–18.0 GHz) [43]. It is very interesting that three fluctuations appear in the frequency range of 2.0–6.0, 6.0–12.0, and 12.0–18.0 GHz in the ε'' curves of all six samples, which implies there may be potential resonances in the corresponding frequency range. These resonances, that have been confirmed to be beneficial for microwave absorption, are usually attributed to various polarization relaxations, including ionic polarization, electronic polarization, dipole orientation polarization, and interfacial polarization (space charge polarization) [44–48]. Besides electronic polarization, ionic polarization can also be excluded due to its ultrahigh frequency response (10^3–10^6 GHz) [43]. Dipole orientation polarization generally dissipates electromagnetic energy by frequency dispersion, because the dipoles present in the system cannot reorient themselves along with the applied electric field [42, 49]. However, these cobalt assemblies do not produce any signs of frequency dispersion, and thus interfacial polarization should be responsible for the multiple resonances [38, 44]. When an external alternating electric field is applied, the different electron distributions between hcp-cobalt and fcc-cobalt will lead to the uneven charge distribution at the interfaces (i.e., stacking faults) and consequent distorted electric moments, which can further account for the loss of incident electromagnetic waves. That is why a strong and broad peak in the range of 12.0–18.0 GHz only appears in the samples with proper phase composition (Co-350, Co-400, and Co-450), but disappears in the samples with overwhelming fcc phase (Co-500 and Co-550).

Different from the complex permittivity, the real parts of complex permeability are less affected by the phase composition (Fig. 4c), which may be related to the comparable saturated magnetization of these cobalt assemblies (Fig. 3). However, it is found that their imaginary parts of complex permeability are greatly distinguishable (Fig. 4d). From Co-300 to Co-500, the μ'' values are continuously increased, particularly Co-500 gives its variation between 0.28 and 0.5 in the whole frequency range, indicating its considerable magnetic loss ability. Co-550 presents similar μ'' values to Co-500. Based on these results, it can be concluded that fcc-cobalt is conducive to the formation of stronger magnetic loss than hcp-cobalt. It has been reported that magnetic loss mainly originates from hysteresis, domain wall resonance, natural ferromagnetic resonance, and eddy current effect [50]. However, hysteresis loss and domain wall resonance loss can be easily excluded, because the former is negligible in the weak field and the latter usually occurs at much lower frequency (MHz) [51]. With respect to the eddy current loss, it can be evaluated by the following equation (Eq. 1),

$$\mu'' = 2\pi\mu_0(\mu')^2\sigma \cdot d^2f \big/ 3, \qquad (1)$$

where σ (S m^{-1}) is the electrical conductivity and μ_0 (H m^{-1}) is the permeability in vacuum. If the reflection loss results from the eddy current effect, the values of C_0 ($C_0 = \mu''(\mu')^{-2}f^{-1}$) will be constant and independent on the frequency [52]. Figure S6 demonstrates that the values of C_0 for these Co assemblies continuously change from 2.0 to 18.0 GHz, confirming the rather limited contribution from the eddy current loss. That is to say, the natural ferromagnetic resonance is the primary reason for the magnetic loss of these cobalt assemblies. The dielectric loss tangent (tan $\delta_e = \mu''/\mu'$) and the magnetic loss tangent (tan $\delta_m = \varepsilon''/\varepsilon'$) are two common concepts to evaluate the dielectric loss and magnetic loss abilities, respectively. As shown in Fig. 4e, f, tanδ_e and tanδ_m interpret the similar results to complex permittivity and complex permeability, where Co-350 possesses superior dielectric loss ability, and Co-500 and Co-550 are the candidates with the best magnetic loss ability.

The reflection loss properties for incident electromagnetic wave are calculated using the measured complex permittivity and permeability according to the transmission line theory [53],

$$R_L(\text{dB}) = 20 \log \left| \frac{Z_{in} - 1}{Z_{in} + 1} \right| \qquad (2)$$

Figure 5 Reflection loss curves of various cobalt assemblies with absorbers thickness of 1 mm in the frequency range of 2.0–18.0 GHz (**a**), and absorber thickness-dependent reflection loss of Co-400 in the frequency range of 2.0–18.0 GHz (**b**).
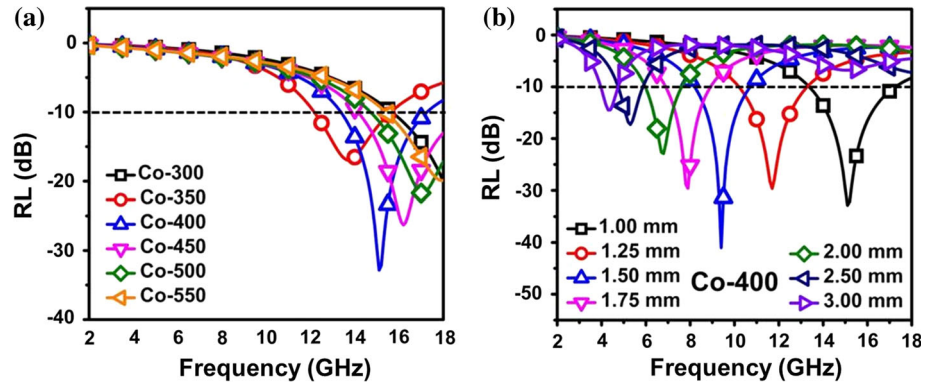
Z_{in} refers to the normalized input impedance of a metal-backed microwave absorbing layer and is given by,

$$Z_{in} = \sqrt{\frac{\mu_r}{\varepsilon_r}}\tanh\left[j\left(\frac{2\pi}{c}\right)fd\sqrt{\mu_r\varepsilon_r}\right], \tag{3}$$

where ε_r and μ_r are the complex permittivity and permeability, respectively, of the composite medium, c is the velocity of electromagnetic waves in free space, f is the microwave frequency, and d is the thickness of an absorber. Figure 5a shows the calculated results of frequency-dependent reflection loss properties of various cobalt assemblies with an absorber thickness of 1.0 mm in the frequency range of 2.0–18.0 GHz. Although all cobalt assemblies can work for the consumption of incident electromagnetic waves, their specific performances are greatly distinguishable and very sensitive to the phase composition. The minimum values of reflection loss for Co-300, Co-350, Co-400, Co-450, Co-500, and Co-550 are −20.0 dB at 18.0 GHz, −17.0 dB at 13.8 GHz, −32.8 dB at 15.1 GHz, −26.3 dB at 16.2 GHz, −21.7 dB at 17.0 GHz, and −19.9 dB at 17.9 GHz, respectively, and the corresponding effective bandwidths over −10.0 dB (90% absorption) of these cobalt assemblies are 2.5 GHz (15.5–18.0 GHz), 3.6 GHz (12.1–15.7 GHz), 4.0 GHz (13.3–17.3 GHz), 3.9 GHz (14.1–18.0 GHz), 3.3 GHz (14.7–18.0 GHz), and 2.6 GHz (15.4–18.0 GHz), respectively. In the field of microwave absorption, reflection loss and response bandwidth are two important reference points for an eligible microwave absorber, and thus Co-400 herein may be taken as the best candidate in this series. It is very surprising that neither Co-350 with superior dielectric loss ability nor Co-500/Co-550 with the strongest magnetic loss ability produces the best reflection loss properties. This is because the

microwave absorption cannot be determined only by complex permittivity and permeability, and there is another important parameter, the concept of matched characteristic impedance, relating to the reflection loss properties of microwave absorbers. In general, the matching of characteristic impedance greatly depends on the relationship between complex permittivity and complex permeability, and an overly large difference between complex permittivity and complex permeability is not favorable for the matching of characteristic impedance and results in considerable reflections of the incident electromagnetic wave at the surface of absorbers [40, 54]. Ma et al. have ever proposed a delta-function method to validate the impedance matching degree of various absorbers by the following equation [55],

$$|\Delta| = \left|\sinh^2(Kfd) - M\right|, \tag{4}$$

where K and M are determined by the complex permittivity and complex permeability,

$$K = \frac{4\pi\sqrt{\mu'\varepsilon'} \cdot \sin\frac{\delta_e + \delta_m}{2}}{c \cdot \cos\delta_e \cos\delta_m} \tag{5}$$

$$M = \frac{4\mu'\cos\delta_e\varepsilon'\cos\delta_m}{(\mu'\cos\delta_e - \varepsilon'\cos\delta_m)^2 + \left[\tan\left(\frac{\delta_m}{2} - \frac{\delta_e}{2}\right)\right]^2(\mu'\cos\delta_e + \varepsilon'\cos\delta_m)^2}. \tag{6}$$

The smaller delta value means better impedance matching. Figure S7 shows the calculated delta value maps of Co-300, Co-350, Co-400, Co-450, Co-500, and Co-550. It is obvious that Co-400 has larger area close to zero ($|\Delta| \leq 0.2$) than other cobalt assemblies, especially when the absorber thickness is relatively thin, which can directly explain the superior reflection loss properties of Co-400.

According to Eq. (3), the thickness (d) of absorbers can also affect the reflection loss, and thus the

Table 1 Microwave absorbing properties of various cobalt absorbers in previous references and this work

Absorbers	Phase	Thickness (mm)	Min RL (Frequency)	Bandwidth over −10 dB (range, GHz)	Integrated thickness (mm)	Bandwidth over −10 dB (range, GHz)	Ref.
Sword-like Co	hcp–fcc	1.0	−9.9 dB (18.0 GHz)	–	1.0–3.0	13.0 (5.0–18.0)	7
Co flakes	hcp	1.0	−12.0 dB (11.0 GHz)	1.2 (10.8–12.0)	0.8–2.0	9.5 (5.0–14.5)	13
Co superstructures	hcp–fcc	1.0	−20.0 dB (18.0 GHz)	2.0 (16.0–18.0)	1.0–3.0	13.5 (4.5–18.0)	15
Co dendrites	hcp–fcc	1.0	−20.0 dB (12.5 GHz)	2.5 (11.5–14.0)	1.0–2.0	9.2 (4.8–14.0)	16
Flower-like Co	hcp	1.0	−25 dB (16.2 GHz)	3.3 (14.7–18.0)	1.0–3.0	10.1 (4.0–8.5, 12.4–18.0)	22
Co dendrites	hcp–fcc	1.0	−10.0 dB (18.0 GHz)	–	1.0–3.0	11.0 (5.0–16.0)	23
Co nanowires	hcp	1.0	−2.5 dB (6.5 GHz)	–	1.0–3.0	–	24
Porous Co rods	hcp	1.0	−25.0 dB (17.5 GHz)	2.7 (15.2–18.0)	1.0–1.6	9.0 (9.0–18.0)	30
Co microflowers	hcp	1.0	−11.0 dB (13.2 GHz)	1.5 (12.5–14.0)	1.0–3.0	11.0 (3.0–14.0)	56
Co nanoplatelets	hcp–fcc	1.0	12.5 dB (11.4 GHz)	2.3 (10.2–12.5)	1.0–3.0	9.5 (3.0–12.5)	57
Co-400	hcp–fcc	1.0	−32.8 dB (5.1 GHz)	4.0 (13.3–17.3)	1.0–3.0	13.4 (4.0–17.4)	Herein

relationship between the thickness and the reflection loss of Co-400 is further investigated (Fig. 5b). The microwave frequency corresponding to the maximum reflection loss shifts negatively with the increase of thickness, and a minimum of −41.0 dB at 9.4 GHz can be achieved when the thickness is 1.5 mm. Besides, the value of reflection loss exceeding −10.0 dB can be obtained in the range 4.0–17.4 GHz with a variation in thickness from 1.0 to 3.0 mm. The strong reflection loss over such wide frequency ranges further suggests that Co-400 will be a promising microwave absorber, whose absorption band can be modulated simply by manipulating the thickness to satisfy applications in different frequency bands. In Table 1, we list the reflection loss properties of some typical metal cobalt absorbers that are measured from similar conditions, and it is clear that the excellent performance of Co-400 in this work is indeed superior to most of them. This significant enhancement can be attributed to two aspects: (1) the phase compositions in Co-400 are rationally optimized, and thus the matching of characteristic impedance can be effectively improved (Fig. S7), while the effect of crystalline phase in the cobalt absorbers in Table 1 is neglected, even in those with randomly mixed phases [7, 15, 16, 23, 57]; (2) the rich porous structure of Co-400 will promote the multiple reflections and repeated consumption of incident electromagnetic wave [32, 33]. In order to further address the contribution of porous structure to microwave absorption, a control sample (Co-control) is also prepared by reducing commercial cobalt oxide. The Rietveld refinement of XRD pattern reveals that the proportions of hcp and fcc phases in Co-control are 5.8 and 94.2% (Fig. S8), respectively, which are very close to those of Co-550 (Fig. 2). Co-control presents dense agglomeration with negligible porous microstructure (Fig. S9). It is very interesting that the different microstructure endows Co-control with distinguishable electromagnetic functions, where its complex permittivity (including real parts and imaginary parts) is remarkably enhanced and its complex permeability is less impacted (Fig. S10a, b). These changes result in the drastically weakened microwave absorption properties of Co-control (Fig. S10c). This can be attributed to the fact that the overly large difference between complex permittivity and complex permeability pushes the sample of Co-control into the region of impedance mismatch. That is to say, porous structure in Co assemblies also works for the matching of characteristic impedance. These results demonstrate that rational design on both microstructure and phase composition will be a better choice for enhanced performance of cobalt-based microwave absorbers.

Conclusions

With cobalt oxalate (CoC_2O_4) as a self-sacrificing precursor template, porous cobalt assemblies have been successfully prepared through an in situ hydrogen reduction. The obtained cobalt assemblies inherit the basic microstructure from their precursor,

and possess abundant pores due to the release of gaseous species. XRD results demonstrate that these cobalt assemblies are composed of hcp phase and fcc phase, and their composition can be easily controlled by manipulating the reduction temperature. It is very interesting that the electromagnetic functions of hcp-phase cobalt and fcc-phase cobalt are quite different, where the former favors good dielectric loss and the latter results in strong magnetic loss. The optimum phase composition will endow these porous cobalt assemblies with well-matched characteristic impedance and excellent microwave absorption. The superiority of porous cobalt assemblies can be further manifested from a comparison to some typical cobalt absorbers previously reported. These results demonstrate that rational design on both microstructure and phase composition will be more helpful to upgrade the microwave absorption of metal cobalt, and also provide an indication for the fabrication of high-performance cobalt-based micro-wave absorbers in the future.

Acknowledgements

Electronic supplementary material: The online version of this article (doi:10.1007/s10853-016-0687-9) contains supplementary material, which is available to authorized users.

References

[1] Puntes VF, Krishnan KM, Alivisatos AP (2001) Colloidal nanocrystal shape and size control: the case of cobalt. Science 291:2115–2117

[2] Anagnostopoulou E, Grindi B, Lacroix LM, Ott F, Panagiotopoulos I, Viau G (2016) Dense arrays of cobalt nanorods as rare-earth free permanent magnets. Nanoscale 8:4020–4029

[3] den Breejen JP, Sietsma JR, Friedrich H, Bitter JH, de Jong KP (2010) Design of supported cobalt catalysts with maximum activity for the Fischer–Tropsch synthesis. J Catal 270:146–152

[4] Kumar VA, Gupta RK, Murty SN, Prasad AD (2016) Hot workability and microstructure control in $Co_{20}Cr_{15}W_{10}Ni$ cobalt-based superalloy. J Alloy Compd 676:527–541

[5] Sachet E, Schubert WD, Mühlbauer G, Yukimura J, Kubo Y (2012) On the formation and in situ observation of thin surface layers of cobalt on sintered cemented carbides. Int J Refract Met Hard Mater 31:96–108

[6] Wang ZZ, Bi H, Wang PH, Wang M, Liu ZW, Shen L, Liu XS (2015) Magnetic and microwave absorption properties of self-assemblies composed of core–shell cobalt–cobalt oxide nanocrystals. Phys Chem Chem Phys 17:3796–3801

[7] Wen S, Zhao X, Liu Y, Cheng J, Li H (2014) Synthesis of hierarchical sword-like cobalt particles and their microwave absorption properties. RSC Adv 4:40456–40463

[8] Shi XL, Cao MS, Yuan J, Fang XY (2009) Dual nonlinear dielectric resonance and nesting microwave absorption peaks of hollow cobalt nanochains composites with negative permeability. Appl Phys Lett 95:163108

[9] Sun S, Murray CB (1999) Synthesis of monodisperse cobalt nanocrystals and their assembly into magnetic superlattices. J Appl Phys 85:4325–4330

[10] Dinega DP, Bawendi MG (1999) A solution-phase chemical approach to a new crystal structure of cobalt. Angew Chem Int Edit 38:1788–1791

[11] de PR Moreira I, Roldán A, Illas F (2010) Electronic and magnetic structure of bulk cobalt: the α, β, and ε-phases from density functional theory calculations. J Chem Phys 133:024701

[12] Sort J, Surinach S, Munoz JS, Baró MD, Wojcik M, Jedryka E, Nadolski S, Sheludko N, Nogués J (2003) Role of stacking faults in the structural and magnetic properties of ball-milled cobalt. Phys Rev B 68:014421

[13] Wang ZZ, Bi H, Wang M, Wang PH, Liu XS (2015) High microwave permittivity and resonance–antiresonance electromagnetic behaviors of flake-shaped cobalt microcrystals. Mater Chem Phys 159:173–177

[14] Wang XL, Shi GM, Shi FN, Xu G, Qi YY, Li D, Zhang ZD, Zhang YJ, You HP (2016) Synthesis of hierarchical cobalt dendrites based on nanoflake self-assembly and their microwave absorption properties. RSC Adv 6:40844–40853

[15] Wen SL, Liu Y, Zhao XC, Fan ZZ (2015) Synthesis, permeability resonance and microwave absorption of flake-assembled cobalt superstructure. J Magn Magn Mater 385:182–187

[16] Liu T, Zhou PH, Xie JL, Deng LJ (2011) The hierarchical architecture effect on the microwave absorption properties of cobalt composites. J Appl Phys 110:033918

[17] Wen SL, Liu Y, Zhao XC (2015) Facile chemical synthesis, electromagnetic response, and enhanced microwave

absorption of cobalt powders with controllable morphologies. J Chem Phys 143:084707

[18] He CZ, Qiu S, Wang XZ, Liu JR, Luan LQ, Liu W, Itoh M, Machida KI (2012) Facile synthesis of hollow porous cobalt spheres and their enhanced electromagnetic properties. J Mater Chem 22:22160–22166

[19] Wang C, Han XJ, Zhang XL, Hu SR, Zhang T, Wang JY, Du YC, Wang XH, Xu P (2010) Controlled synthesis and morphology-dependent electromagnetic properties of hierarchical cobalt assemblies. J Phys Chem C 114:14826–14830

[20] Wen SL, Liu Y, Zhao XC, Cheng JW, Li H (2014) Synthesis, dual-nonlinear magnetic resonance and microwave absorption properties of nanosheet hierarchical cobalt particles. Phys Chem Chem Phys 16:18333–18340

[21] Ma F, Qin Y, Li YZ (2010) Enhanced microwave performance of cobalt nanoflakes with strong shape anisotropy. Appl Phys Lett 96:202507

[22] Tong GX, Yuan JH, Wu WH, Hu Q, Qian HS, Li LC, Shen JP (2012) Flower-like Co superstructures: morphology and phase evolution mechanism and novel microwave electromagnetic characteristics. CrystEngComm 14:2071–2079

[23] Wen SL, Liu Y, Zhao XC, Cheng JW (2014) Optimal microwave absorption of hierarchical cobalt dendrites enhanced by multiple dielectric and magnetic resonance. J Appl Phys 116:054310

[24] Chen WB, Han MG, Deng LJ (2010) High frequency microwave absorbing properties of cobalt nanowires with transverse magnetocrystalline anisotropy. Physica B 405:1484–1488

[25] Zhao HT, Zhang B, Zhang JS, Zhang LF, Han XJ, Xu P, Zhou Y (2010) Field-assisted synthesis and electromagnetic properties of aligned magnetic nanostructures by γ-irradiation induced reduction. J Phys Chem C 114:21214–21218

[26] Wen SL, Liu Y, Zhao XC (2015) The hierarchical three-dimensional cobalt superstructure: controllable synthesis, electromagnetic properties and microwave absorption. Adv Powder Technol 26:1520–1528

[27] Qiao ZA, Brown SS, Adcock J, Veith GM, Bauer JC, Payzant EA, Unocic RR, Dai S (2012) A topotactic synthetic methodology for highly fluorine-doped mesoporous metal oxides. Angew Chem Int Edit 124:2942–2947

[28] Zhao HT, Du YC, Kang LL, Xu P, Du L, Sun ZH, Han XJ (2013) Precursor-directed synthesis of quasi-spherical barium ferrite particles with good dispersion and magnetic properties. CrystEngComm 15:808–815

[29] Tong GX, Liu Y, Cui TT, Li YN, Zhao YT, Guan JG (2016) Tunable dielectric properties and excellent microwave absorbing properties of elliptical Fe$_3$O$_4$ nanorings. Appl Phys Lett 108:072905

[30] Kong J, Wang F, Wan X, Liu J, Itoh M, Machida KI (2012) Template-free synthesis of Co nanoporous structures and their electromagnetic wave absorption properties. Mater Lett 78:69–71

[31] Pujol O, Bowen P, Stadelmann PA, Hofmann H (2004) Growth and self-assembly of nanostructured CoC$_2$O$_4$·2H$_2$O particles. J Phys Chem B 108:13128–13136

[32] Zhou JH, He JP, Li GX, Wang T, Sun D, Ding XC, Zhao JQ, Wu SC (2010) Direct incorporation of magnetic constituents within ordered mesoporous carbon-silica nanocomposites for highly efficient electromagnetic wave absorbers. J Phys Chem C 114:7611–7617

[33] Du YC, Liu T, Yu B, Gao HB, Xu P, Wang JY, Wang XH, Han XJ (2012) The electromagnetic properties and microwave absorption of mesoporous carbon. Mater Chem Phys 135:884–891

[34] Muñoz-Tabares JA, Bejtka K, Lamberti A, Garino N, Bianco S, Quaglio M, Pirri CF, Chiodoni A (2016) Nanostructural evolution of one-dimensional BaTiO$_3$ structures by hydrothermal conversion of vertically aligned TiO$_2$ nanotubes. Nanoscale 8:6866–6876

[35] Pun GP, Mishin Y (2012) Embedded-atom potential for hcp and fcc cobalt. Phys Rev B 86:134116

[36] Ogo SH, Shimizu T, Nakazawa Y, Mukawa K, Mukai D, Sekine Y (2015) Steam reforming of ethanol over K promoted Co catalyst. Appl Catal A 495:30–38

[37] Kong LT, Zhang RF, Li ZC, Liu BX (2003) Magnetic properties of Co and Co-Ag alloys in equilibrium/nonequilibrium structures studied by ab initio calculations. Phys Rev B 68:134446

[38] Qiang R, Du YC, Chen DT, Ma WJ, Wang Y, Xu P, Ma J, Zhao HT, Han XJ (2016) Electromagnetic functionalized Co/C composites by in situ pyrolysis of metal-organic frameworks (ZIF-67). J Alloy Compd 681:384–393

[39] Leslie-Pelecky DL, Rieke RD (1996) Magnetic properties of nanostructured materials. Chem Mater 8:1770–1783

[40] Du YC, Liu WW, Qiang R, Wang Y, Han XJ, Ma J, Xu P (2014) Shell thickness-dependent microwave absorption of core-shell Fe$_3$O$_4$@C composites. ACS Appl Mater Interfaces 6:12997–13006

[41] Wen B, Cao MS, Hou ZL, Song WL, Zhang L, Lu MM, Jin HB, Fang XY, Wang WZ, Yuan J (2013) Temperature dependent microwave attenuation behavior for carbon-nanotube/silica composites. Carbon 65:124–139

[42] Wang Y, Du YC, Qiang R, Tian CH, Xu P, Han XJ (2016) Interfacially engineered sandwich-like rGO/carbon microspheres/rGO composite as an efficient and durable microwave absorber. Adv Mater Interfaces 3:1500684

[43] Tian CH, Du YC, Xu P, Qiang R, Wang Y, Ding D, Xue JL, Ma J, Zhao HT, Han XJ (2015) Constructing uniform core–

shell PPy@PANI composites with tunable shell thickness toward enhancement in microwave absorption. ACS Appl Mater Interfaces 7:20090–20099

[44] She W, Bi H, Wen ZW, Liu QH, Zhao XB, Zhang J, Che RC (2016) Tunable microwave absorption frequency by aspect ratio of hollow polydopamine@α-MnO$_2$ microspindles studied by electron holography. ACS Appl Mater Interfaces 8:9782–9789

[45] Liu XG, Li B, Geng DY, Cui WB, Yang F, Xie ZG, Kang DJ, Zhang ZD (2009) (Fe, Ni)/C nanocapsules for electromagnetic-wave-absorber in the whole Ku-band. Carbon 47:470–474

[46] Liu J, Cao WQ, Jin HB, Yuan J, Zhang DQ, Cao MS (2015) Enhanced permittivity and multi-region microwave absorption of nanoneedle-like ZnO in the X-band at elevated temperature. J Mater Chem C 3:4670–4677

[47] Lv HL, Liang XH, Cheng Y, Zhang HQ, Tang DM, Zhang BS, Ji GB, Du YW (2015) Coin-like α-Fe$_2$O$_3$@CoFe$_2$O$_4$ core-shell composites with excellent electromagnetic absorption performance. ACS Appl Mater Interfaces 7:4744–4750

[48] Qiang R, Du YC, Zhao HT, Wang Y, Tian CH, Li ZG, Han XJ, Xu P (2015) Metal organic framework-derived Fe/C nanocubes toward efficient microwave absorption. J Mater Chem A 3:13426–13434

[49] Ohlan A, Singh K, Chandra A, Dhawan SK (2010) Microwave absorption behavior of core-shell structured poly (3, 4-ethylenedioxy thiophene)-barium ferrite nanocomposites. ACS Appl Mater Interfaces 2:927–933

[50] Lu B, Dong XL, Huang H, Zhang XF, Zhu XG, Lei JP, Sun JP (2008) Microwave absorption properties of the core/shell-type iron and nickel nanoparticles. J Magn Magn Mater 320:1106–1111

[51] Wu MZ, Zhang YD, Hui S, Xiao TD, Ge SH, Hines WA, Budnick JI, Taylor GW (2002) Microwave magnetic properties of Co$_{50}$/(SiO$_2$)$_{50}$ nanoparticles. Appl Phys Lett 80:4404–4406

[52] Liu QH, Cai Q, Zhao XB, Bi H, Wang C, Wu DS, Che RC (2015) Insights into size-dominant magnetic microwave absorption properties of CoNi microflowers via off-axis electron holography. ACS Appl Mater Interfaces 7:4233–4240

[53] Cui CK, Du YC, Li TH, Zheng XY, Wang XH, Han XJ, Xu P (2012) Synthesis of electromagnetic functionalized Fe$_3$O$_4$ microspheres/polyaniline composites by two-step oxidative polymerization. J Phys Chem B 116:9523–9531

[54] Cao MS, Qin RR, Qiu CJ, Zhu J (2003) Matching design and mismatching analysis towards radar absorbing coatings based on conducting plate. Mater Des 24:391–396

[55] Ma Z, Zhang Y, Cao CT, Yuan J, Liu JB (2011) Attractive microwave absorption and the impedance match effect in zinc oxide and carbonyl iron composite. Physica B 406:4620–4624

[56] Ma Z, Liu QF, Yuan J, Wang ZK, Cao CT, Wang JB (2012) Analyses on multiple resonance behaviors and microwave reflection loss in magnetic Co microflowers. Phys Status Solidi B 249:575–580

[57] Li JG, Huang JJ, Qin Y, Ma F (2007) Magnetic and microwave properties of cobalt nanoplatelets. Mater Sci Eng B 138:199–204